

## Scanning SQUID microscopy of sparsely twinned $\text{YBa}_2\text{Cu}_3\text{O}_{7-\delta}$

Kathryn A. Moler

*Department of Physics, Princeton University, Princeton, New Jersey 08544*

John R. Kirtley

*IBM T. J. Watson Research Center, Yorktown Heights, New York 10598*

Ruixing Liang, Douglas Bonn, and Walter N. Hardy

*Department of Physics, University of British Columbia, Vancouver, British Columbia V6T1Z1*

(Received 4 October 1996)

Magnetic images of two sparsely twinned  $\text{YBa}_2\text{Cu}_3\text{O}_{7-\delta}$  single crystals were taken in low applied magnetic fields ( $H_a < 100$  mG) with a scanning SQUID microscope. The SQUID sensors have 4 or 8  $\mu\text{m}$  pickup loops and a magnetic flux resolution of  $10^{-3}hc/2e$  under normal operating conditions. The images showed Meissner screening with a large demagnetization factor and isolated trapped vortices. The trapped vortices carried integral ( $hc/2e$ ) magnetic flux and were much smaller than the spatial resolution of the sensor. At this level of resolution, there was no evidence for unusual magnetic features, such as fractional vortices, associated with the twin boundaries. [S0163-1829(97)01417-3]

### I. INTRODUCTION

Magnetic flux penetrates superconductors as fluxoids quantized in units of  $\Phi_0 = hc/2e$ . This quantization results from the requirement that the order parameter be single valued, and applies to the magnetic flux in rings and in superconducting quantum interference Devices (SQUID's), as well as to vortices in Josephson junctions and in type-II superconductors. The possibility of nonintegral vortices was first suggested for rotational vortices in  $\text{He}^3$ , where the order parameter has nontrivial phases.<sup>1</sup> Such nonintegral vortices could also show up in superconductors which contain interfaces such as Josephson junctions and grain boundaries, either because of unconventional properties of the junction<sup>2</sup> or because of an unconventional order parameter.<sup>3,4</sup> For example, a  $d$ -wave order parameter changes sign (a phase change of  $\pi$ ) under a  $90^\circ$  rotation. In the right geometry, this phase change results in a spontaneously generated half-integral flux quantum,  $\Phi_0/2$ , both theoretically<sup>3,4</sup> and experimentally.<sup>5</sup>

Fractional vortices, which for this paper will mean fractions other than half-integral ( $\Phi_0/2$ ), have not been definitively observed. Recently Kirtley *et al.* reported distinct areas of localized flux with magnitudes much less than  $\Phi_0$  in scanning SQUID microscope measurements of biepitaxial grain boundary junctions that completely enclosed hexagonal and triangular regions of  $\text{YBa}_2\text{Cu}_3\text{O}_{7-\delta}$  (YBCO).<sup>6</sup> It was difficult to draw definite conclusions from these measurements because the instrumental spatial resolution, Josephson penetration depth, and lengths of the grain boundaries used in these measurements were all about the same size. Mannhart and coworkers showed that very similar effects are observed in asymmetric  $45^\circ$  bicrystal grain boundaries, and argued that these effects could result from a  $d_{x^2-y^2}$  gap symmetry when the roughness of the grain boundary is considered.<sup>7</sup>

The unambiguous observation of isolated vortices carry-

ing a fraction (other than  $1/2$ ) of a flux quantum would imply phase changes in the order parameter of other than  $\pi$ , and could only result from a complex order parameter, breaking time-reversal symmetry.<sup>8,9</sup> Sigrist *et al.* have suggested that a complex order parameter may develop locally on the twin boundaries of YBCO.<sup>10</sup> They speculate that as an orthorhombic order parameter ( $d + \epsilon s$ ) rotates across a twin boundary (from  $d + \epsilon s$  to  $d - \epsilon s$ ),<sup>11</sup> it may be energetically favorable for  $\epsilon$  to become imaginary rather than zero. The gradient in the phase of the order parameter near the twin boundary should result in equal currents flowing in opposite directions on either side of the twin boundary. The order parameter at the twin boundary may be either  $d + i\epsilon s$  or  $d - i\epsilon s$ . If both states existed in different sections of the twin boundaries, fractional vortices would form at the domain wall between the two regions.

Several phase-sensitive Josephson experiments demonstrate the existence of a sign change in the order parameter of YBCO,<sup>5,12-15</sup> including tunneling experiments in Pb-YBCO corner junctions in which the phase change is inferred from the critical current,<sup>13</sup> and imaging experiments which show half-integral flux quanta in tricrystal geometries of YBCO.<sup>5,12</sup> These experiments point towards the particular pairing symmetry  $d_{x^2-y^2}$ .<sup>16</sup> There are also  $c$ -axis tunneling experiments, however, in which the detection of first-order tunneling in a  $c$ -axis YBCO-Pb junction seems to indicate that the order parameter of YBCO cannot be purely  $d$  wave.<sup>17,18</sup> At first glance the orthorhombicity of YBCO provides a natural reconciliation of these experiments: if the order parameter is  $d + \epsilon s$ , then the dominant  $d$ -wave order parameter would result in the in-plane  $\pi$  phase shift while the  $s$ -wave component would allow  $c$ -axis tunneling. However, the  $c$ -axis experiments have been performed both on untwinned samples and on heavily twinned samples. The twinning should result in strongly suppressed tunneling and, depending on the number and distribution of twin boundaries, in unusual Fraunhofer diffraction patterns such as

those observed in corner junctions<sup>13</sup> and in 45° grain boundaries.<sup>7</sup> While there is some decrease in the  $I_c R$  value for the heavily twinned samples, the decrease is not as large as one would guess, and the unusual Fraunhofer diffraction patterns have not been observed. As Sigrist *et al.* pointed out, the existence of a time-reversal symmetry breaking order parameter on twin boundaries would reconcile these experiments, since the  $s$ -wave order parameter of the lead could couple into the order parameter on the twin boundaries.<sup>10</sup>

In this paper, we report on the results of a search for magnetic signatures of complex order parameters near twin boundaries using scanning SQUID microscopy in optimally doped and underdoped YBCO. The observation of fractional vortices would be an unambiguous signature of a complex order parameter. Since such vortices result from a boundary between two complex order parameters, such as  $d+i\epsilon s$  and  $d-i\epsilon s$ , their absence does not rule out time-reversal symmetry breaking. In contrast, currents flowing along the twin boundary must exist even if there is only a single complex order parameter at the twin boundary, but it is difficult to estimate the magnitude of these currents *a priori*. Neither signature was observed, setting weak limits on local time-reversal symmetry breaking near the twin boundaries.

## II. SAMPLES

$\text{YBa}_2\text{Cu}_3\text{O}_{7-\delta}$  single crystals were grown by a flux-growth technique in  $\text{BaZrO}_3$ -coated yttria stabilized zirconia crucibles and annealed on YBCO ceramic in a tube furnace under high purity oxygen flow.<sup>19</sup> The pressure and temperature required to achieve particular doping levels had been previously calibrated and checked by titration on ceramic samples. Crystals grown by this technique have been characterized by low-field magnetization,  $ab$ -plane resistivity, heat capacity, and microwave surface resistance. Similar samples show a linear temperature dependence of the microwave penetration depth.<sup>20</sup>

This study required twin boundaries which were isolated on the length scale of the SQUID imaging. Two crystals were chosen which had regions of naturally sparse twin boundary spacing and clean surfaces. A sketch of one crystal, indicating the relatively densely twinned areas, is shown in Fig. 1(a). Although much of the crystals were densely twinned, some regions of each crystal had isolated twin boundaries which were more than 10  $\mu\text{m}$  from the nearest neighboring boundaries. The twin boundaries were oriented at 45° to the edges of the crystal. Both crystals were studied at both optimum doping ( $7-\delta=6.95$ ,  $T_c=93.1$  K) and underdoping ( $7-\delta=6.60$ ,  $T_c=60$  K).

## III. TECHNIQUE

Images were obtained using a Scanning SQUID Microscope (SSM) at 4.2 K. The sensor was mounted on a flexible cantilever and mechanically scanned relative to the sample. The pickup loop was located several microns away from the tip of the sensor chip, which rested physically on the sample. The plane of the pickup loop made a shallow angle ( $\sim 20^\circ$ ) with the sample. The spatial resolution is limited by the size of the pickup loop (4 or 8  $\mu\text{m}$ ), and by the distance

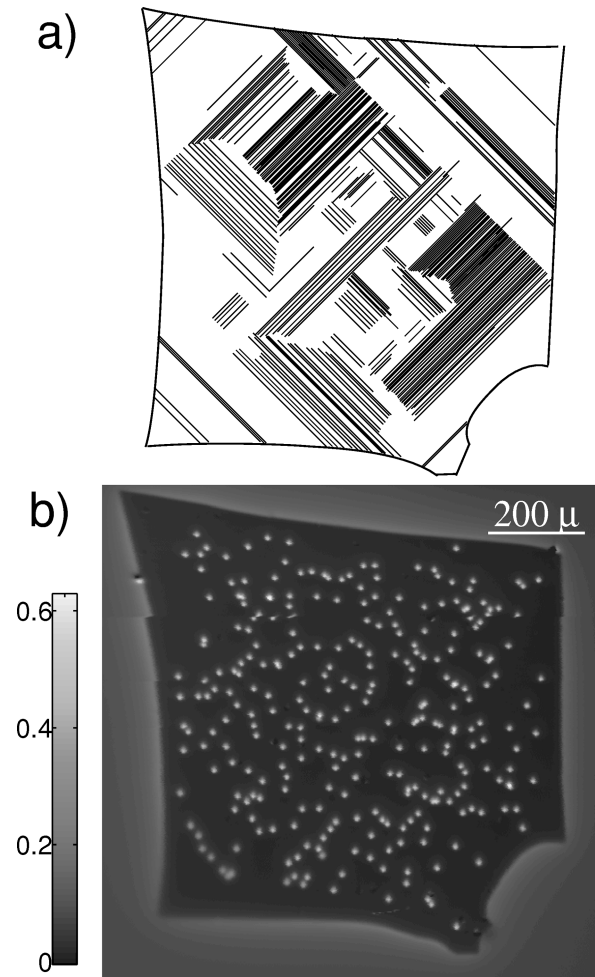


FIG. 1. (a) Sketch indicating the distribution and orientation of twins in a sparsely twinned  $\text{YBa}_2\text{Cu}_3\text{O}_{6.95}$  crystal. Not all twins are shown. (b) Scanning SQUID microscope image of this crystal, cooled in an applied magnetic field of about 10 mG.

between the pickup loop and the sample (about 2  $\mu\text{m}$ ). Since the signal is proportional to the total flux through the pickup loop, the images show the perpendicular magnetic field a few microns above the surface of the sample convoluted with the geometry of the pickup loop. The SSM has been more completely described elsewhere.<sup>21</sup>

Although the SQUID's have a noise of  $2 \times 10^{-6} \Phi_0 / \sqrt{\text{Hz}}$ , under normal scanning conditions the noise of the SSM is dominated by other factors. The digitization noise is  $2 \times 10^{-4}$  full scale, where the full scale is usually several  $\Phi_0$  or less. Also, surface roughness inductively couples to the pickup loop. These two factors result in an effective noise, defined as the standard deviation of the background signal in regions with no clear magnetic features, of  $10^{-3} \Phi_0$  under the conditions of this study. The surface roughness can also lead to potential systematic errors by changing the orientation of the SQUID pickup loop with respect to the surface.

## IV. RESULTS

Figure 1(b) shows an SSM image of an optimally doped YBCO crystal, cooled in a field of about 10 mG. The edges

of the crystal are clearly visible, since the local magnetic field immediately outside the crystal is larger than the background magnetic field. The actual crystal is rectangular except at one corner, but the image is slightly distorted by nonlinearities in the scan.

Previous work on similar crystals has shown that  $H_{c1} = 1100$  G at 4 K for fields applied parallel to the  $c$  axis.<sup>22</sup> Despite the fact that the applied field is much less than either  $H_{c1}$  or the geometry-dependent first penetration field, there are many vortices trapped inside the crystal. At 4 K, the number of vortices in the interior does not change with changing magnetic field for the small fields ( $< 1$  G) used in this study. Presumably, the fact that vortices are observed in the sample at fields so far below  $H_{c1}$  is an indication of the high pinning potential in these materials.

Aside from some flux expulsion, which occurs over a distance less than  $100 \mu\text{m}$  from the edge of the crystal, the density of trapped vortices closely follows the field which is applied during cooling divided by  $\Phi_0$ . This occurs in all of the cuprates studied, for thin films as well as single crystals, and appears to be independent of the shape of the sample. These observations indicate that the vortices each have  $hc/2e$  flux trapped in them, in agreement with previous work.<sup>23</sup>

There are several magnetic dipoles appearing in the Fig. 1(b) image. Similar dipoles have also appeared in other images of other superconductors, including films of various high- $T_c$  materials and niobium films. These dipoles are correlated with topographical features on the surface, probably  $\text{BaCuO}_x$  flux spots, which are visible under optical inspection. The apparent magnetic dipoles may result from the SQUID sensor “rocking” as it passes over the features.

More detail may be seen in two  $512 \mu\text{m} \times 512 \mu\text{m}$  closeups of the central region of the crystal (Fig. 2). These images were taken in different cooldowns with an  $8 \mu\text{m}$  square pickup loop and a  $4 \mu\text{m}$  octagonal pickup loop, with one data point per  $\mu\text{m}$ . The main results are the uniformity of the vortices in both spatial extent and total flux, and the lack of any clear feature associated with the twin boundaries. Closeups of vortices chosen at random (Fig. 3) show that the vortices have a uniform appearance within the limits of the imaging technique, and that the apparent size and shape of the vortices is determined by the size and shape of the pickup loop.

The in-plane penetration depth in similar crystals has been shown to be  $\lambda_L = 0.15 \mu\text{m}$ ,<sup>24</sup> much less than the size of the SQUID pickup loop. It is thus expected that the images in Fig. 3 will be consistent with vortices which are essentially point sources, unless there are two or more neighboring fractional vortices contributing to each flux maximum. On length scales long compared to the London penetration depth but small compared to the size of the crystal, a vortex can be modeled as a monopole source of magnetic field,<sup>25</sup> so that the  $z$  component of the field is given by  $B_z = \Phi_0 z / 2\pi r^3$ . This field can be integrated over the SQUID’s pickup loop to give the expected magnetic flux signal. Figure 4(a) shows the result of this calculation, neglecting the tilt of the pickup loop with respect to the sample, for an  $8 \mu\text{m}$  square pickup loop at a height of  $2.5 \mu\text{m}$  above the surface. The calculation is compared with cross sections of the magnetic flux data from

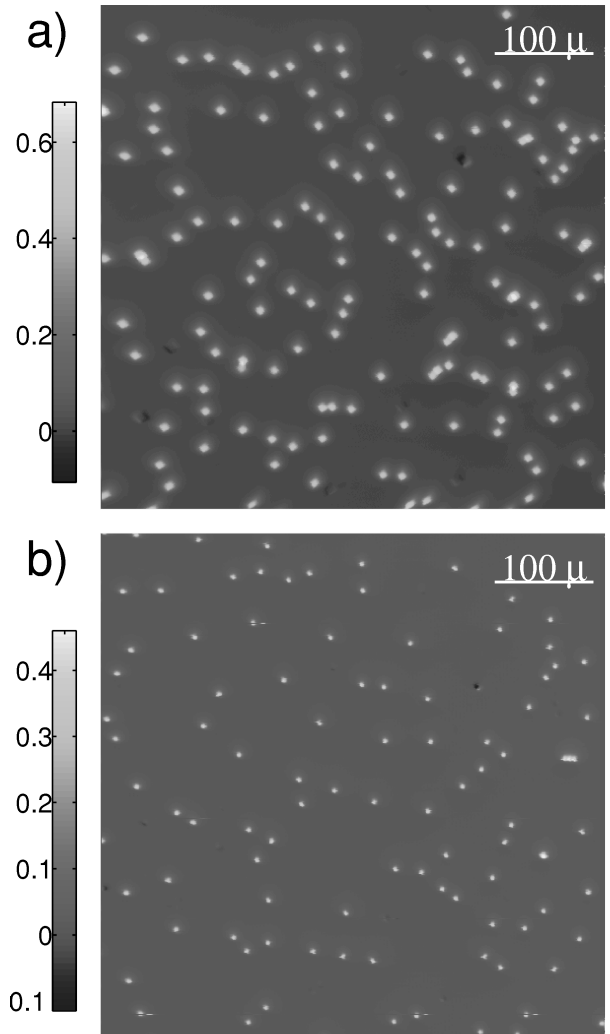


FIG. 2. Magnetic images taken during separate cooldowns with different pickup loops: (a)  $8 \mu\text{m}$  pickup loop, (b)  $4 \mu\text{m}$  pickup loop.

the vortices in Figs. 3(b)–3(d). Figure 4(b) shows the calculated flux for the  $4 \mu\text{m}$  octagonal loop at a height of  $1.5 \mu\text{m}$ , compared with cross sections of the magnetic flux data from the vortices in Figs. 3(f)–3(h). The heights of the pickup loops have been treated as the only free parameter, and the resulting heights are consistent with the geometry of the SQUID sensors.

There do not appear to be any fractional vortices in these images. It is possible that what appears to be a single integral vortex may actually be two or more fractional vortices, whose flux sums to one flux quantum, which are too close to be resolved by the SQUID pickup loop. In order to indicate time-reversal symmetry breaking, such vortices must be isolated, that is, they must be far apart compared to a London penetration depth. As an example of the difficulty of resolving such vortices, Fig. 4(c) shows a calculation of the flux through the  $4 \mu\text{m}$  octagonal SQUID pickup loop for two half-integral vortices separated by 0, 2, 4, or  $6 \mu\text{m}$ . Conservatively, the images in Fig. 3 are not sufficient to resolve vortices which are separated by less than the size of the pickup loop. However, if different sets of fractional vortices were separated by different amounts, then there would be a

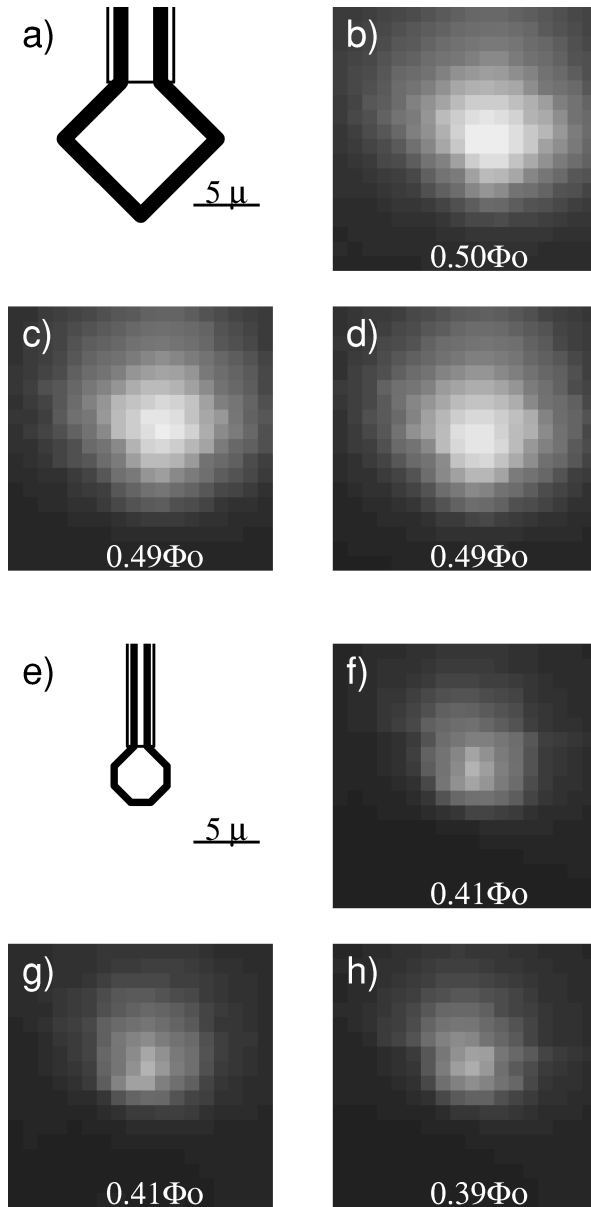


FIG. 3. (a) Sketch of the  $8\ \mu\text{m}$  pickup loop. (b)–(d) Closeups of individual vortices from Fig. 2(a), imaged with the  $8\ \mu\text{m}$  pickup loop. (e) Sketch of the  $4\ \mu\text{m}$  pickup loop. (f)–(h) Closeups of individual vortices from Fig. 2(b), imaged with the  $4\ \mu\text{m}$  pickup loop. Labels indicate the maximum flux through the pickup loop of each vortex.

corresponding spread in the maxima in Fig. 2.

A histogram of the flux maxima (Fig. 5) thus serves to quantify the uniformity of the vortices, and the possibility that separated fractional vortices appear as one integral vortex. For this purpose, a maximum is defined as a data point that is at least three standard deviations above the local background and is larger than its eight nearest neighbors. Note that the  $x$  axis on Fig. 5, flux through the SQUID pickup loop, is not the same as the total flux carried by the vortex. The peaks at  $0.5\Phi_0$  in Fig. 5(a) and  $0.4\Phi_0$  in Fig. 5(b) represent integral vortices, which has been confirmed by cooling in various applied magnetic fields and counting the number

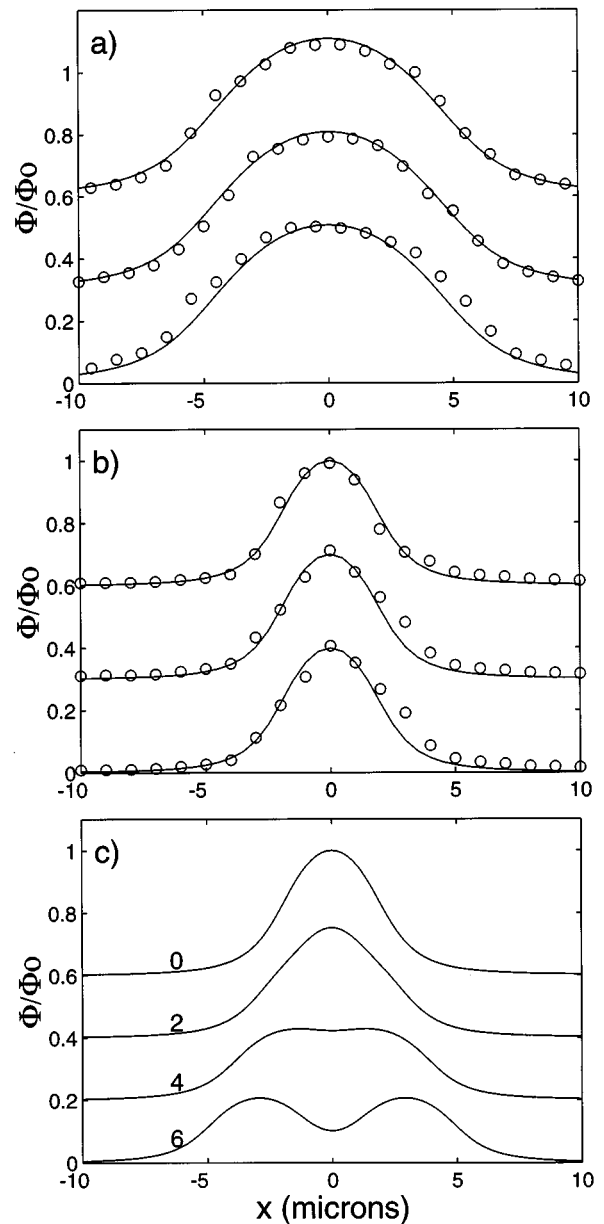


FIG. 4. (a) Calculated flux through the  $8\ \mu\text{m}$  pickup loop scanning over a single vortex at a height of  $2.5\ \mu\text{m}$ , compared with cross sections of the three vortices in Figs. 3(b)–3(d). (b) Calculated flux through the  $4\ \mu\text{m}$  pickup loop scanning over a single vortex at a height of  $1.5\ \mu\text{m}$ , compared with cross sections of the three vortices in Figs. 3(f)–3(h). (c) Calculated flux through the  $4\ \mu\text{m}$  pickup loop scanning at a height of  $1.5\ \mu\text{m}$  above two half-integral vortices separated by 0, 2, 4, and  $6\ \mu\text{m}$ . Curves have been offset for clarity, by  $0.3\Phi_0$  in (a) and (b) and by  $0.2\Phi_0$  in (c).

of trapped vortices. A few maxima in Fig. 5 result from one of the dipoles, mentioned above, which we believe result from bumps on the surface. A maximum resulting from a single isolated pixel, whose neighboring pixels are within the background, cannot be taken to represent an actual magnetic feature, which should have a spatial extent of at least the SQUID pickup loop diameter. None of the maxima which are below  $0.1\Phi_0$  meet this criteria. The peaks in Fig. 5 thus represent integral vortices with a spread of a few percent, which is consistent with the sampling density of  $1\ \mu\text{m}$  per

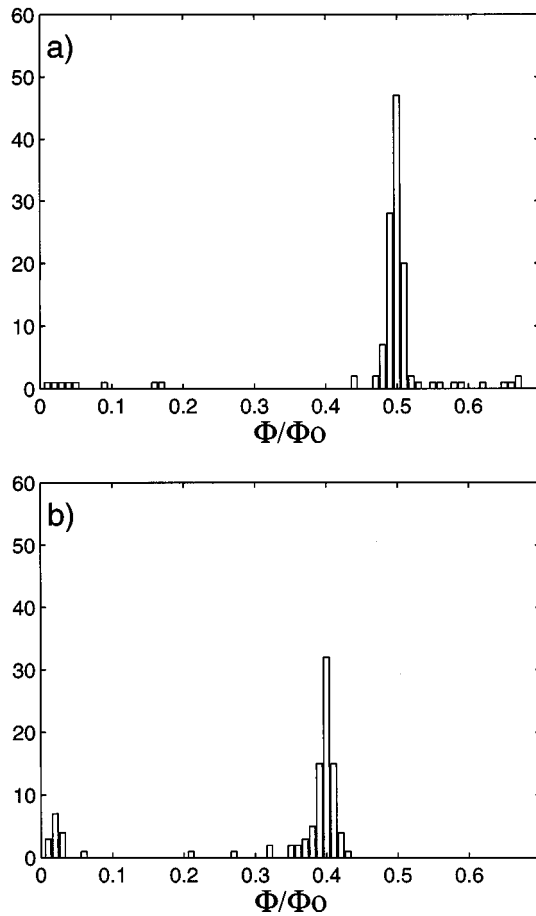


FIG. 5. Distribution of local maxima in data sets taken with (a) the  $8\ \mu\text{m}$  pickup loop and (b) the  $4\ \mu\text{m}$  pickup loop.

data point. This result suggests that any pairs or triplets of fractional vortices are closer than about a  $\mu\text{m}$ .

In images taken in higher magnetic fields than the ones shown here, the vortices appear to sit preferentially in more heavily twinned regions or near twin boundaries. Otherwise, there is no clear magnetic feature associated with the twin boundaries, as can be seen from an image taken in nominally zero applied magnetic field [Figs. 6(a) and 6(b)].

There is no evidence for currents flowing near the twin boundaries, which would be expected to exist over a length scale of the London penetration depth. Since the London penetration depth is small compared to the size of the pickup loop, and the currents on opposite sides of the twin boundary would flow in opposite directions, it may be that the magnetic field from the currents averages to a flux which is below the sensor resolution. As an extremely crude model for the magnetic field from such currents, we take one-dimensional infinite wires located a distance  $\lambda_L = 0.15\ \mu\text{m}$  to each side of the twin boundary, carrying currents flowing in opposite directions. While currents associated with the twin boundaries would be expected to be strips as thick as the crystal rather than wires at the surface, the magnetic field from currents which are much more than a penetration depth would be shielded by the bulk of the crystal. Modeling the twin boundaries as two current-carrying wires is only intended to indicate the scale of the possible magnetic fields.

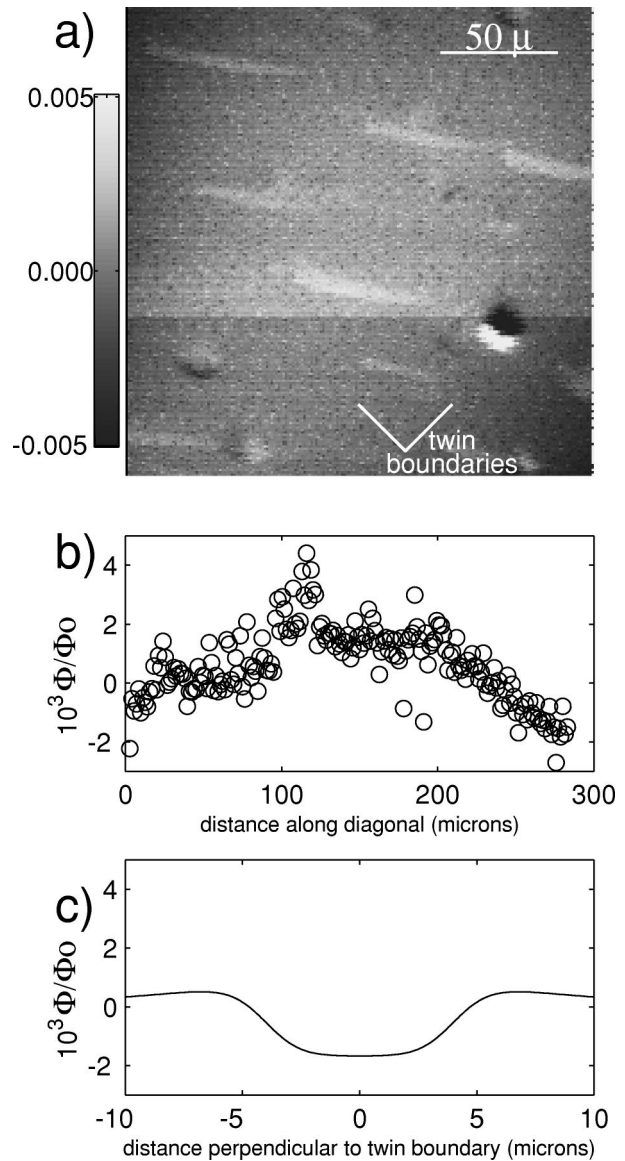


FIG. 6. (a) A magnetic image taken with the  $8\ \mu\text{m}$  pickup loop in nominally zero applied magnetic field, with a linear background signal subtracted. The lines indicate the direction of the twin boundaries. (b) Diagonal cross section through the image starting from lower left. (c) Calculated flux through the  $8\ \mu\text{m}$  pickup loop for a crude model of the twin boundaries: two wires separated by  $2\lambda_L = 0.30\ \mu\text{m}$ , carrying opposing currents  $j_c\lambda_L^2 \approx 20\ \mu\text{A}$ .

Guessing a current of  $I = j_c\lambda_L^2 \approx 20\ \mu\text{A}$ , where  $j_c \approx 10^5\ \text{A}/\text{cm}^2$  is the critical current density, and integrating over an  $8\ \mu\text{m}$  square SQUID loop scanning at a height of  $2.5\ \mu\text{m}$ , results in the flux profile in Fig. 5(b). Although no such signal is seen in these images, more realistic models would probably result in an even smaller signal, and cannot be ruled out with the present data.

The structure of the twin boundaries are known to be quite sensitive to oxygen content. With the assumption that the detailed behavior of the rotation of the orthorhombic order parameter would also be sensitive to oxygen content, the measurements were repeated on underdoped crystals. This paper has concentrated on data obtained for one optimally doped crystal. Quantitatively similar results were obtained

on a second optimally doped crystal, and on both crystals after reoxygenation to  $7 - \delta = 6.60$ .

### V. DISCUSSION

Several limits have been set on the possibility of unusual magnetic features associated with the twin boundaries in  $\text{YBa}_2\text{Cu}_3\text{O}_{6.95}$  and  $\text{YBa}_2\text{Cu}_3\text{O}_{6.60}$ . The vortices have been shown to carry uniform integrally quantized flux within a few percent. If isolated fractional vortices exist on the twin boundaries, they carry flux which is less than  $\sim 10^{-3}\Phi_0$ . If two or more fractional vortices carrying a total flux of  $1\Phi_0$  are sufficiently close together to appear to be an integral vortex, then they are located about a micron or less apart from each other. Opposing currents which flow along oppo-

site sides of the twin boundaries and vary on a length scale of  $\lambda_L$  must be carrying a current which is less than  $20 \mu\text{A}$  within a London penetration depth of the surface.

No magnetic features which indicate the formation of a complex order parameter on the twin boundary have been observed. To rule out the magnetic features associated with such a complex order parameter, however, would require measurements with probes of comparable flux sensitivity to the present sensors, but with a spatial resolution of order the London penetration depth.

### ACKNOWLEDGMENTS

We thank J. Berlinsky, R. B. Laughlin, M. Sigrist, and C. C. Tsuei for useful discussions.

- 
- <sup>1</sup>G. E. Volovik and V. P. Mineev, JETP Lett. **24**, 561 (1976).  
<sup>2</sup>V. B. Geshkenbein and A. I. Larkin, JETP Lett. **43**, 395 (1986).  
<sup>3</sup>V. B. Geshkenbein, A. I. Larkin, and A. Barone, Phys. Rev. B **36**, 235 (1987).  
<sup>4</sup>M. Sigrist and T. M. Rice, J. Phys. Soc. Jpn. **61**, 4283 (1992).  
<sup>5</sup>J. R. Kirtley, C. C. Tsuei, M. Rupp, J. Z. Sun, L. S. Yu-Jahnes, A. Gupta, M. B. Ketchen, K. A. Moler, and M. Bhushan, Phys. Rev. Lett. **76**, 1336 (1996).  
<sup>6</sup>J. R. Kirtley, P. Chaudhari, M. B. Ketchen, N. Khare, Shawn-Yu Lin, and T. Shaw, Phys. Rev. B **51**, 12 057 (1995).  
<sup>7</sup>J. Mannhart, H. Hilgenkamp, B. Mayer, Ch. Gerber, J. R. Kirtley, K. A. Moler, and M. Sigrist, Phys. Rev. Lett. **77**, 2782 (1996).  
<sup>8</sup>M. R. Beasley, D. Lew, and R. B. Laughlin, Phys. Rev. B **49**, 12 330 (1994).  
<sup>9</sup>M. Sigrist, D. B. Bailey, and R. B. Laughlin, Phys. Rev. Lett. **74**, 3249 (1995).  
<sup>10</sup>M. Sigrist, K. Kuboki, P. A. Lee, A. J. Millis, and T. M. Rice, Phys. Rev. B **53**, 2835 (1996).  
<sup>11</sup>As pointed out by M. B. Walker, experiments on highly twinned crystals suggest that the phase of the  $d$ -wave component of the order parameter locks across a twin boundary, M. B. Walker, Phys. Rev. B **53**, 5835 (1996).  
<sup>12</sup>C. C. Tsuei, J. R. Kirtley, C. C. Chi, S. Yu-Jahnes, A. Gupta, T. Shaw, J. Z. Sun, and M. B. Ketchen, Phys. Rev. Lett. **73**, 593 (1994).  
<sup>13</sup>D. A. Wollman, D. J. Van Harlingen, J. Giapintzakis, and D. M. Ginsberg, Phys. Rev. Lett. **74**, 797 (1995); D. A. Wollman, D. J. Van Harlingen, W. C. Lee, D. M. Ginsberg, and A. J. Leggett, *ibid.* **71**, 2134 (1993).  
<sup>14</sup>D. A. Brawner and H. R. Ott, Phys. Rev. B **50**, 6530 (1994).  
<sup>15</sup>A. Mathai, Y. Gim, R. C. Black, A. Amar, and F. C. Wellstood, Phys. Rev. Lett. **74**, 4523 (1995).  
<sup>16</sup>J. F. Annett, N. Goldenfeld, and A. J. Leggett, J. Low Temp. Phys. **105**, 473 (1996).  
<sup>17</sup>R. Kleiner, A. S. Katz, A. G. Sun, R. Summer, D. A. Gajewski, S. H. Han, S. I. Woods, E. Dantsker, B. Chen, K. Char, M. B. Maple, and R. C. Dynes, Phys. Rev. Lett. **76**, 2161 (1996); A. G. Sun, D. A. Gajewski, M. B. Maple, and R. C. Dynes, *ibid.* **72**, 2267 (1994).  
<sup>18</sup>R. Kleiner, A. S. Katz, A. G. Sun, R. Summer, D. A. Gajewski, S. H. Han, S. I. Woods, E. Dantsker, B. Chen, K. Char, M. B. Maple, R. C. Dynes, and John Clarke, Phys. Rev. Lett. **76**, 2161 (1996).  
<sup>19</sup>Ruixing Liang, P. Dosanjh, D. A. Bonn, D. J. Baar, J. F. Carolan, and W. N. Hardy, Physica C **195**, 51 (1992).  
<sup>20</sup>W. N. Hardy, D. A. Bonn, D. C. Morgan, Ruixing Liang, and Kuan Zhang, Phys. Rev. Lett. **70**, 3999 (1993).  
<sup>21</sup>J. R. Kirtley, M. B. Ketchen, C. C. Tsuei, J. Z. Sun, W. J. Gallagher, Lock See Yu-Jahnes, A. Gupta, K. G. Stawiasz, and S. J. Wind, IBM J. Res. Dev. **39**, 655 (1995).  
<sup>22</sup>Ruixing Liang, P. Dosanjh, D. A. Bonn, W. N. Hardy, and A. J. Berlinsky, Phys. Rev. B **50**, 4212 (1994).  
<sup>23</sup>P. L. Gammel, D. J. Bishop, G. J. Dolan, J. R. Kwo, C. A. Murray, L. F. Schneemeyer, and J. V. Waszczak, Phys. Rev. Lett. **59**, 2952 (1987).  
<sup>24</sup>T. M. Riseman, J. H. Brewer, K. H. Chow, W. N. Hardy, R. F. Kiefl, S. R. Kretzman, R. Liang, W. A. MacFarlane, P. Mendels, and G. Morris, Phys. Rev. B **52**, 10 569 (1995).  
<sup>25</sup>A. M. Chang, H. D. Hallen, H. F. Hess, H. L. Kao, J. Kwo, A. Sudbo, and T. Y. Chang, Europhys. Lett. **20**, 645 (1992).